Long-duration Experiments Assessing Atomic Oxygen Effects on Thin Polyimides

Elena A. Plis[1], Ryan Ramirez[2], Anthony Semenova[2], Daniel M. Hewett[3], David B. Oakes[3], and Heather M. Cowardin[4]
[1]Georgia Tech Research Institute (GTRI), Atlanta, GA, 30318, USA
[2]Georgia Institute of Technology, Atlanta, GA, 30318, USA
[3]Physical Sciences Inc. 20 New England Business Center Andover, MA 01810-1077
[4]NASA Orbital Debris Program Office, NASA Johnson Space Center, 2101 NASA Pkwy., Houston, TX 77058, USA
{elena.plis}@gtri.gatech.edu

***Abstract*—The destructive impact of atomic oxygen (AO) on spacecraft in near-Earth orbits can lead to significant erosion and mass loss of spacecraft materials. Structural supports, thermal control systems, and coatings containing organic polymers are particularly susceptible to high-velocity AO attacks, resulting in material degradation and surface roughening. This wear progressively compromises the structural integrity and operational efficiency of the spacecraft. Furthermore, AO-induced damage can weaken spacecraft structures, increasing the risk of debris generation under specific conditions. Therefore, a comprehensive understanding of material behavior under space conditions is essential to predict fragmentation and mitigate space debris. This study involves long-duration experiments to evaluate the effects of AO on various types of thin polymer films.**

I. Introduction

Space, particularly in low Earth orbit (LEO), is strategically vital as it supports essential infrastructure for modern life, enhances national security capabilities, and paves the way for future exploration and sustainable development. The destructive impact of AO on spacecraft within near-Earth altitudes has been extensively documented by the scientific community, beginning with early space shuttle missions [1]. The high reactivity of AO, coupled with the exacerbated erosive potential due to the high velocities of spacecraft in LEO, can result in considerable erosion and mass loss, particularly on polymer surfaces. This can progressively impair the spacecraft's structural integrity and operational efficiency. In addition, material erosion and surface roughening due to AO can weaken spacecraft structures, potentially increasing the risk of debris generation under certain conditions.

Debris is a form of space pollution that can have severe consequences for commercial and other activities in outer space. Launching satellites and conducting operations in orbit inevitably generate various types of orbital debris, which can collide with functional satellites, sometimes with disastrous results [2]. Even small pieces of debris, despite their small mass, can cause catastrophic damage due to their high velocities [3]–[5]. Furthermore, space debris is self-propagating, as scenario where collisions lead to a cascading chain reaction of further collisions.

Orbital space debris originates from various sources, including remnants of launch vehicles and rocket bodies, defunct satellites, fragmentation of satellites and rocket bodies [7], and even tools lost by astronauts [8].

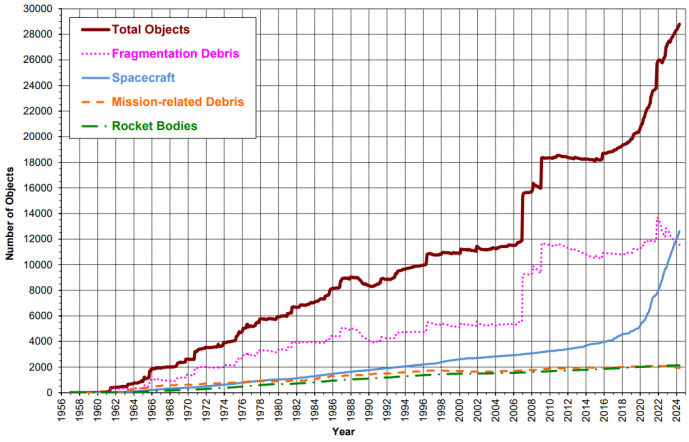

Fig. 1. Historical increase of the orbital debris tracked by US Space Surveillance Network (SSN) [9]

Figure 1 shows that the amount of debris formed by pieces generated when satellites or other space objects break apart due to collisions, explosions, or structural failures has increased over time, until 2024 when the number of spacecraft due to the prolific number of constellations overcame these trending numbers. Significant spikes in the amount of fragmentation debris occurred due to China's direct-ascent anti-satellite (ASAT) test on Fengyun-1C in 2007, the accidental collision between Cosmos 2251 and Iridium 33 in 2009, and Russia's ASAT test in November 2021. Thus, an in-depth understanding of how materials behave under space conditions is critical in anticipating the likelihood of fragmentation and other processes that contribute to the growing issue of space debris.

Proc. 9th European Conference on Space Debris, Bonn, Germany, 1–4 April 2025, published by the ESA Space Debris Office
Editors: S. Lemmens, T. Flohrer & F. Schmitz, (http://conference.sdo.esoc.esa.int, April 2025)

blank Kapton®, Kapton® coated with a thin indium tin oxide (ITO) antistatic layer to mitigate plasma charging in orbit, and breadboard model (BBM) material intended to be used for an in situ sensor. Additionally, these materials were perforated to simulate micrometeoroid orbital debris (MMOD) impacts to further characterize material degradation.

II. Methodology

A. Materials

The studied materials detailed in Table I, in their unperforated state, were received from NASA's Orbital Debris Program Office. Three types of materials were investigated, namely, 0.5 mil thick Kapton® manufactured by Sheldahl, serving as a baseline; ITO-coated Kapton®; and BBM. The 12 µm ITO coating was deposited on both sides of 0.5 mil thick Kapton® coupons. The BBM consists of a conductive grid sheet (copper etched on Kapton®) nominally 0.5 mil thick. The BBM samples exhibited three types of conditions: edge damage; surface damage; and intact, as used in US government FY18 hypervelocity impact tests.

TABLE I
Tested Materials

Material Type	Size W x L (cm x cm)	Quantity
Blank Kapton®	3 x 3	3
ITO-coated Kapton®	3 x 3	3
BBM	9 x 9	3

B. Material Perforation

To further characterize material degradation, especially when the underlying material with the ITO coating has been exposed to AO, material coupons were perforated to simulate MMOD impacts. Puncture tests were performed using needles of specific diameters. In the first puncture test, a needle with a diameter of 1059 µm was used to completely perforate the materials, with a piece of supporting cardboard ensuring full penetration through the sample to mimic the clean blow of large MMOD through the material. For the second puncture test, a needle of the same diameter (1059 µm) was pressed perpendicularly to the surface of the sample, but the materials were not completely perforated, mimicking debris rebounding from the surface. In a third puncture test, a needle with a diameter of 885.6 µm was used and the materials were completely perforated, using a supporting cardboard piece to facilitate needle penetration – similar to the technique used in the first puncture test – for punctures caused by smaller MMOD. Representative images of needle punctures for each puncture test performed are shown in Figure 2.

For each type of material studied, one coupon was perforated using a single puncture technique at five different loca-

Fig. 2. The representative images of needle punctures for each puncture test conducted. Images were taken using a Keyence 3D optical microscope.

C. AO Exposure

AO exposure was performed using the FAST® source at the Physical Sciences Inc. (PSI) in accordance with ASTM-E2089-15. The samples were arranged on the exposure mounting plate, as seen in Figure 3, using a double-sided tape known to not leave any residue. The BBM samples were cut into 3 cm x 3 cm pieces with edge and surface damage preserved. Also arranged on the mounting plate were 11 Kapton H® 'witness' samples. These witness samples are used to calculate the O-atom fluence for each material test sample by averaging their surrounding witness samples using the known density of Kapton® H (1.427 g/cm^3) and the LEO erosion yield (3×10^{-24} cm^3/O-atom).

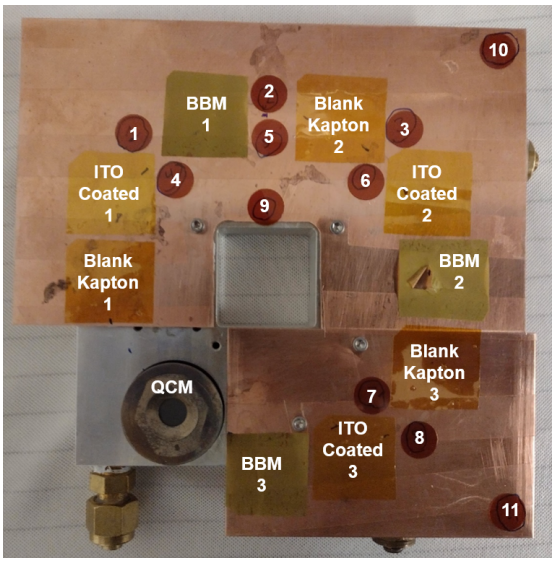

Prior to AO exposure, the prepared mounting plate was placed in the vacuum chamber overnight to allow the samples to desorb any absorbed atmospheric moisture. The materials were subsequently subjected to 1,457,690 pulses of oxygen atoms traveling at 8 km/s for a total duration of 135 hours, while maintaining a temperature of 25°C, equivalent to 18 months of sample exposure to LEO environment. Effective peak atomic oxygen fluence during the run was $1.8(\pm 0.2) \times 10^{21}$ O atoms/cm^2.

D. Material Characterization Methods

1) Mass Loss: Prior to AO exposure, all samples were placed in a vacuum chamber overnight to remove any absorbed water. Each sample was then weighed using a microbalance, and these weights were recorded at multiple time points to account for any water absorption during the transfer from the chamber to the scale. During this test, the laboratory humidity was approximately 45% and significant water absorption was observed in most samples both before and after AO exposure. The 'dry' masses were estimated from the mass measurements taken over time after removal from the vacuum.

2) Surface Analysis: Surfaces were examined before and after AO exposure, with special attention given to the morphology of the punctured holes. Root mean square (RMS) surface roughness was measured using the Keyence VHX-7000 digital microscope to assess erosion effects on both pristine and exposed samples. Measurements were taken at a sampling area of approximately 0.42 mm^2 per shot. To minimize the impact of outliers, each measurement was processed with a Gaussian filter and an L-filter value of 0.25 mm and 50 mm, respectively, to remove the largest surface elements. A total of three measurements were taken at random, distinct locations on each sample.

III. Results

During the AO exposure, all blank Kapton® samples eroded completely, whereas the ITO-coated samples maintained their integrity despite becoming fragile. The BBM samples experienced significant erosion, with the fibrous matrix underneath remaining largely intact, but the filler material eroding substantially.

A. Blank Kapton® Samples

All studied blank Kapton® test coupons eroded completely halfway through the AO exposure (1.0×10^{21} O-atoms/ cm^2), leaving nothing for post-exposure testing.

Using the published erosion rate of Kapton® by 5 eV atomic oxygen at 3×10^{-24} cm^3/O-atom, the Kapton® erosion depth, assuming uniform erosion, after exposure to a fluence of 1.0×10^{21} O-atoms/cm^2 is expected to be 30 µm. Since the thickness of the blank Kapton material was 0.5 mil (approx. 12.7 µm),

B. ITO-coated Kapton® Samples

Out of all studied materials, the ITO-coated Kapton® coupons successfully withstood the AO exposure. Figure 4 shows the post-AO-exposure image of the ITO-coated Kapton® sample perforated with a needle of 1059 µm diameter that fully penetrated the material (Sample 1). The sample significantly embrittled due to AO exposure and adhered firmly to the double-sided mounting tape used during the process, making removal impossible.

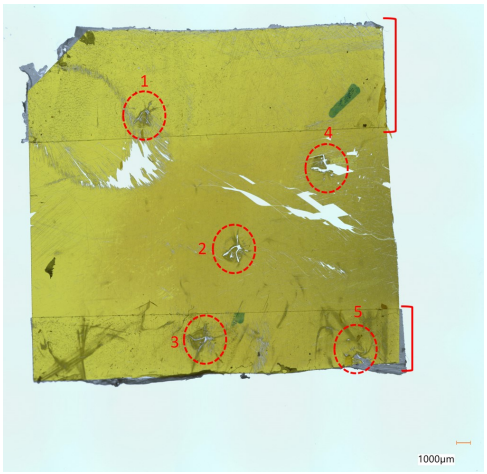

Fig. 4. The post-AO-exposure image of ITO-coated Kapton® (Sample 1) perforated with a needle of 1059 µm diameter that fully penetrated through the sample. Red brackets indicate areas covered with double-sticky tape on the backside used to mount samples on the holder during AO exposure. Five needle punctures are indicated by the dashed red circles numbered 1 - 5.

Among the five punctures, Hole 2 exhibited the least impact from edge effects, unlike Holes 1, 3, and 5 or the AO-induced material fracturing observed in Hole 4. Figure 5 compares optical images of Hole 2 in both pristine and AO-exposed materials. Close-up views (Figure 5b and d) of the AO-exposed material highlight the erosion observed after exposure.

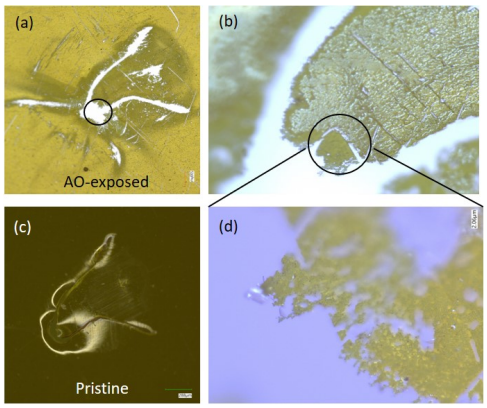

Fig. 5. Optical images of Hole 2 in (a, b, d) AO-exposed and (c) pristine ITO-coated Sample 1 coupon. Close-up views (b and d) of the AO-exposed material highlight the erosion observed after exposure.

Figure 6 shows the post-AO-exposure image of the ITO-coated Kapton® (Sample 2) perforated with a needle of

1, Sample 2 became highly brittle from AO exposure and adherence to the double-sided mounting tape made removal impossible. Among the five punctures, Hole 2 exhibited the least impact from edge effects – unlike Hole 3, which was subject to tape-induced effects (additionally, see Holes 1 and 5), or the AO-induced material tearing observed in Hole 4. Figure 7 compares optical images of Hole 2 in both pristine and AO-exposed materials. A close-up view (Figuer 7c) of the AO-exposed material highlights the erosion observed after exposure.

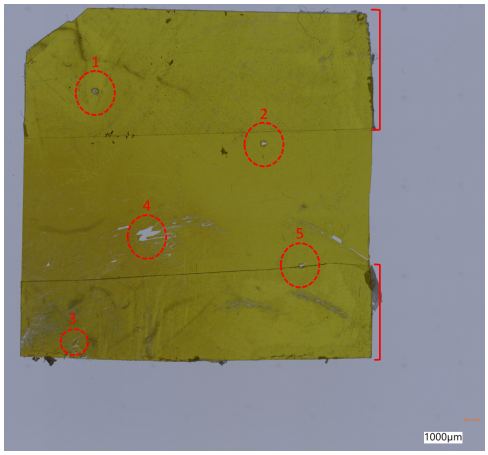

Fig. 6. The post-AO-exposure image of ITO-coated Kapton® perforated with a 1059 µm needle pressed perpendicularly to the sample's surface without fully penetrating the material (Sample 2). Red brackets indicate areas covered with double-sticky tape on the backside used to mount samples on the holder during AO exposure. Five needle punctures are indicated by the dashed red circles and numbers 1 - 5.

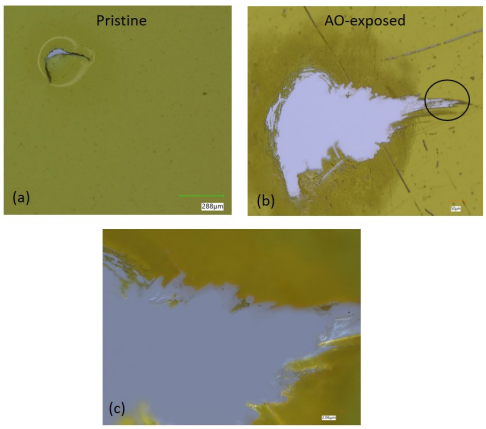

Fig. 7. Optical images of Hole 2 in (a) pristine and (b, c) AO-exposed ITO-coated Sample 2 coupon. Close-up view (c) of the AO-exposed material highlights the erosion observed after exposure.

Finally, Figure 8 shows the post-AO-exposure image of the ITO-coated Kapton® (Sample 3) perforated with a needle of 885.6 µm diameter that fully penetrated the material. Among the studied ITO-coated coupons, this particular sample appeared to be the most affected by the AO bombardment, with significant cracking and erosion sites observed after the of pre- and post-exposure images for a representative puncture, Hole 4.

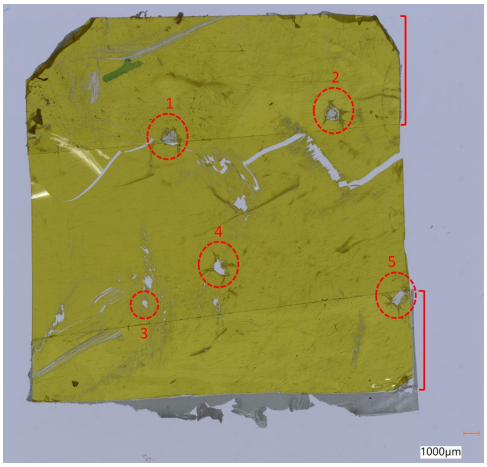

Fig. 8. The post-AO-exposure image of ITO-coated Kapton® perforated with a 885.6 µm needle fully penetrating through the sample (Sample 3). Red brackets indicate areas covered with double-sticky tape on the backside used to mount samples on the holder during AO exposure. Five needle punctures are indicated by the dashed red circles and numbers 1 - 5.

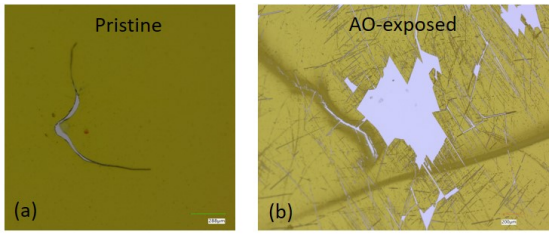

Fig. 9. Optical images of Hole 4 in (a) pristine and (b) AO-exposed ITO-coated Sample 3 coupon.

The summarized damage diameters for each hole in the ITO-coated Kapton®coupons, both before and after AO exposure, are presented in Table 10. There is a general trend of increased hole diameter after AO exposure, with the extent of degradation varied across different coupons and puncture locations. In some cases, the material became so degraded that accurate estimation of post-irradiated hole geometry was not impossible due to tearing or severe damage. For example, in Kapton® ITO-coated Sample 2, punctures performed at sites 3 and 5 showed such extensive damage post-exposure that they were either torn or unmeasurable. The effect of needle diameter and the puncture method variation used during the creation of the holes in different coupons of ITO-coated Kapton® material was not significant compared to the overall AO-induced material degradation.

The measured RMS roughness values of pristine and AO-exposed materials are presented in Table II. The roughness of pristine materials was estimated after the material coupons were perforated, with measurements performed in between puncture sites. Similarly, the roughness of AO-exposed materials was evaluated on unbroken space between perforations.

Sample #	Hole #	Damage diameter (µm)	
		Pristine	AO-exposed
1	1	1482.8	1470.0
	2	1514.1	1501.0
	3	1539.4	1876.2
	4	1466.1	tear
	5	1491.2	hole degraded
Average		1498.74	1,615.7
2	1	351.73	518.1
	2	346.2	589.0
	3	371.8	hole degraded
	4	341.3	tear
	5	368.6	312.0 + tear
Average		355.9	473.0
3	1	1220.2	1214.2
	2	1121.6	1224.0
	3	1280.0	1446.3
	4	1416.4	tear
	5	1437.1	1386.0
Average		1295.1	1,317.6

Fig. 10. The summarized damage diameters for each hole in the ITO-coated Kapton® coupons, both before and after AO exposure.

the roughness did not change significantly, suggesting the effectiveness of the ITO coating for the protection of the polyimide material underneath.

TABLE II
RMS ROUGHNESS VALUES OF PRISTINE AND AO-EXPOSED ITO-COATED KAPTON® COUPONS

Sample	Pristine (µm)	AO-exposed (µm)
1	5.9 ±1.8	12.8 ±3.8
2	4.8 ±1.44	3.4 ±1.02
3	17.7 ±5.3	17.1 ±5.1

C. BBM Samples

Among the three tested BBM coupons, portions of BBM Samples 2 and 3 detached during AO exposure and fell to the chamber floor. The remaining fragments of BBM Sample 1 consisted of copper strands loosely held together by the double-sided tape they were adhered to, as shown in Figure 11. Hence, measurements were unable to be taken due to the complete erosion of filler material.

IV. CONCLUSION

In conclusion, among the studied three types of materials subjected to the peak atomic oxygen fluence of $1.8(\pm 0.2) \times 10^{21}$ O atoms/cm^2, equivalent to approximately 18 months of LEO exposure, the three blank (i.e. uncoated) Kapton® samples were completely eroded, leaving no material for post-exposure analysis. Similarly, the three BBM samples showed significant degradation, with portions of BBM Samples 2 and 3 detaching and falling to the chamber floor during exposure. What remains of BBM Sample 1 consists of loosely bound strands, held together only by the double-sided tape to which they were adhered.

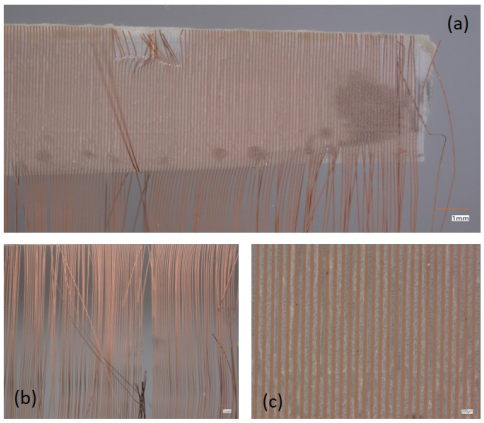

Fig. 11. The optical images of BBM Sample 1 after AO exposure. (a) Eroded region of BBM Sample 1 supported by the mounting tape; close-up views of eroded region (b) with no tape support and (c) supported by the mounting tape.

notable resilience, underscoring the effectiveness of ITO as a protective coating in space environments. The samples became so brittle that they adhered firmly to the mounting tape, making removal impossible. The needle punctures, visibly altered by AO erosion, further emphasized the extent of material degradation. However, the needle diameter and puncture technique had a negligible impact compared to the overall damage caused by AO exposure, with the AO-induced erosion far outweighing any effects from the initial punctures. Surface roughness increased for Sample 1, but remained relatively unchanged for Samples 2 and 3, suggesting localized variations in material response.

ACKNOWLEDGMENTS

This work was supported by NASA Jacobs contract JETS II: PRS23-8331. In addition, this work received partial support from the GTRI Independent Research and Development (IRAD) program and the GTRI Research Internship Program (GRIP).

DISCLAIMERS

Trade names and trademarks are used in this report for identification only. Their usage does not constitute an official endorsement, either expressed or implied, by the National Aeronautics and Space Administration.

REFERENCES

[1] L. Leger, B. Santosmason, J. Visentine, and J. Kuminecz, "Review of low earth orbital (leo) flight experiments," in *Jet Propulsion Lab., Proceedings of the NASA Workshop on Atomic Oxygen Effects*, 1987.
[2] A. Murtaza, S. J. H. Pirzada, T. Xu, and L. Jianwei, "Orbital debris threat for space sustainability and way forward," *IEEE access*, vol. 8, pp. 61 000–61 019, 2020.
[3] D. M. Lear, J. Hyde, E. Christiansen, J. Herrin, and F. Lyons, "Sts-118 radiator impact damage," *NASA Orbital Debris Quart. News*, 2008.
[4] E. L. Christiansen, D. M. Lear, and J. L. Hyde, "Orbital debris quarterly news, october 2014," *Orbital Debris Quarterly News*, vol. 18, no. 4, 2014.
[5] M. J. Neish, M. Takahashi, H. Maejima, H. Kusawake, S. Kawakita, and

[6] D. J. Kessler and B. G. Cour-Palais, "Collision frequency of artificial satellites: The creation of a debris belt," *Journal of Geophysical Research: Space Physics*, vol. 83, no. A6, pp. 2637–2646, 1978.
[7] N. Johnson, "Environmentally-induced debris sources," *Advances in space research*, vol. 34, no. 5, pp. 993–999, 2004.
[8] R. Lea, "Astronauts dropped a tool bag during an ISS spacewalk, and you can see it with binoculars," 2023, accessed: 2024-10-01. [Online]. Available: https://www.space.com/astronauts-international-space-station-tool-bag-visible
[9] "Orbital Debris Quarterly News," vol. 29, no. 1, p. 8, February 2025.